We are IntechOpen, the world's leading publisher of Open Access books Built by scientists, for scientists

6,900
Open access books available

185,000
International authors and editors

200M
Downloads

Our authors are among the

154
Countries delivered to

TOP 1%
most cited scientists

12.2%
Contributors from top 500 universities

WEB OF SCIENCE™

Selection of our books indexed in the Book Citation Index in Web of Science™ Core Collection (BKCI)

Interested in publishing with us?
Contact book.department@intechopen.com

Numbers displayed above are based on latest data collected.
For more information visit www.intechopen.com

Chapter 11

Nonlinear Cascade-Based Control for a Twin Rotor MIMO System

Lidia María Belmonte, Rafael Morales, Antonio Fernández-Caballero and José Andrés Somolinos

Additional information is available at the end of the chapter

http://dx.doi.org/10.5772/64875

Abstract

This research is focused on the development of a nonlinear cascade-based control algorithm for a laboratory helicopter-denominated Twin Rotor MIMO System (TRMS). The TRMS is an underactuated nonlinear multivariable system, characterised by a coupling effect between the dynamics of the propellers and the body structure, which is caused by the action-reaction principle originated in the acceleration and deceleration of the propeller groups. Firstly, this work introduces an extensive description of the platform's dynamics, which was carried out by splitting the system into its electrical and mechanical parts. Secondly, we present a design of a nonlinear cascade-based control algorithm that locally guarantees an asymptotically and exponentially stable behaviour of the controlled generalised coordinates of the TRMS. Lastly, a demonstration of the effectiveness of the proposed approach is provided by means of numerical simulations performed under the MATLAB®/Simulink® environment.

Keywords: nonlinear control, timescale modelling, twin rotor, MIMO systems, laboratory platform

1. Introduction

Currently, there are many possible uses for unmanned aerial vehicles (UAVs), such as inspection operation, battle field operation, forest fire detection, meteorological observation, or search and rescue operation, among others. All these applications require achieving precise control systems. This has motivated an increased interest in the last years from researchers in

INTECH
open science | open minds

© 2016 The Author(s). Licensee InTech. This chapter is distributed under the terms of the Creative Commons Attribution License (http://creativecommons.org/licenses/by/3.0), which permits unrestricted use, distribution, and reproduction in any medium, provided the original work is properly cited. CC BY

developing effective control algorithms for UAVs [1–4]. In many cases, the development of new control strategies requires the use of software and platforms which are able to simulate the operation of the UAVs in order to perform experimental tests for evaluating the different designs. The use of this kind of tools increases the productivity and reduces the development time. For this purpose, different laboratory test rigs have been specifically designed for teaching and research in flight dynamics and control. One such platform is the laboratory helicopter used in this research, namely the Twin Rotor MIMO System (TRMS) [5]. The TRMS is a nonlinear, multivariable and underactuated system, characterised by a coupling effect between the dynamics of the propellers and the body structure, which is caused by the action-reaction principle originated in acceleration and deceleration of the motor-propeller groups. All these features make the control of the TRMS to be perceived as a challenging engineering problem (note that the TRMS, and other laboratory platforms with similar dynamics are more difficult to control than a real helicopter platform [6]). The achievement of an accurate system dynamics model is a challenging problem, whilst, at the same time, an important issue is to develop accurate and efficient control systems.

The development of the dynamic model for the TRMS has been studied by an important number of researches. Ahmad et al. presented mathematical models for the dynamic characterisation of the TRMS, using a black box system identification technique [7] and radial basis function (RBF) networks [8]. Shaheed modelled the dynamics of the TRMS by means of a nonlinear autoregressive process through external input (NARX) approach with a feed-forward neural work and a resilient propagation (RPROP) algorithm [9]. Rahideh and Shaheed have also contributed to the study of the TRMS dynamics by using both Newton- and Lagrange-based methods [10], and two models based on neural networks using Levenberg-Marquardt (LM) and gradient descent (GD) algorithms [11]. Toha and Tokhi presented an adaptive neuro-fuzzy inference system (ANFIS) network design, which was deployed and used for the TRMS modelling [12]. Finally, Tastemirov et al. developed a complete dynamic TRMS model using the Euler-Lagrange method [13].

On the other hand, the design of the control system for the TRMS has been widely discussed through several investigations. Ahmad et al. developed the dynamic model and implemented a feed-forward/open-loop control [14] and a linear quadratic Gaussian control [15]. López-Martínez et al. studied the design of a longitudinal controller based on Lyapunov functions [16], and the application of a nonlinear L_2 controller [17]. Rahideh et al. presented an experimental implementation of an adaptive dynamic nonlinear model inversion control law using artificial neural networks [18]. Other interesting works are those of Tao et al. who designed a parallel distributed fuzzy linear quadratic regulator (LQR) controller [19]. Studies of Reynoso-Meza et al. developed a holistic multi-objective optimisation design technique for controller tuning [20], or the use of a particle swarm optimisation (PSO) algorithm for the proportional-integral-derivative (PID) controller optimisation developed by Coelho et al. [21].

The aim of the present research is to develop a nonlinear cascade-based control algorithm in order to locally guarantee an asymptotically and exponentially stable behaviour of the controlled generalised coordinates of the TRMS. Additionally, the effectiveness of the proposed

http://dx.doi.org/10.5772/64875

nonlinear feedback controller in terms of stabilisation and position tracking performance is demonstrated by means of numerical simulations. Finally, the paper is organised as follows.

Section 2 introduces a description of the TRMS platform by illustrating the details of the dynamics model obtained into two phases: electrical and mechanical parts. Section 3 describes the nonlinear cascade-based controller scheme proposed. The results of the numerical simulations performed under the MATLAB®/Simulink® environment are depicted in Section 4, and, finally, Section 5 is devoted to the conclusions of the work.

2. System description

The TRMS (see **Figure 1**) is a laboratory helicopter platform manufactured by *Feedback Instruments Ltd*©. The TRMS is composed of two propellers that are perpendicular to each other and placed in the extreme of a beam that can rotate freely in both vertical and horizontal planes. Each propeller is driven by a DC motor, thus forming the main and tail rotor of the platform. A main feature of the TRMS is that its movement, unlike a real helicopter, is not achieved by varying the angle of attack of the blades. In this case, the movement of the platform is gotten by means of the variation in the angular velocity of each propeller, which is caused by the change in the control input voltage of each motor.

Figure 1. Twin rotor MIMO system.

This constructive simplification in the TRMS model substantially complicates the dynamics of the system, because a coupling effect between rotors dynamics and the body of the model appears. This effect is caused by the action-reaction principle originated in acceleration and deceleration of the motor-propeller groups.

In addition, the TRMS is an underactuated system. This implies that the number of variables that act as control inputs (voltages applied to the main and the tail rotor; u_m and u_t respectively) is lower than the number of degrees of freedom (DoF) of the system. The DoF are: the pitch (ψ) and the yaw (ϕ) angles, both measured by digital encoders, as well as the angular velocities of the rotors (ω_m for the main rotor and $\omega_t$for the tail), both measured by DC tachometers. Finally, we have to remark that the laboratory platform is locked mechanically, so it cannot move more than ± 2.82 rad in the horizontal plane from -1.05 to $+1.22$ rad in the vertical plane [22]. In other words, $-2.82 \text{ rad} \leq \phi \leq +2.82 \text{ rad}$ and $-1.05 \text{ rad} \leq \psi \leq +1.22 \text{ rad}$.

2.1. Dynamic model of the TRMS

The development of an efficient control algorithm requires a model that represents the dynamic behaviour of the platform under study as accurately as possible. In the particular case of the Twin Rotor MIMO System, the modelling has been addressed from several approaches [7–13]. However, not all of them provide a model that represents the entire complex dynamic behaviour of this experimental platform. For instance, models based on identification techniques have difficulties in representing the effects of coupling, which are characteristic in this platform [7], and neuronal networks and learning algorithms allow obtaining accurate models, but limited to a range of input values and frequencies [11]. Based on previous works developed for the dynamic model of this platform [13, 22–24], a detailed dynamic model of the TRMS has been developed by dividing the whole dynamics of the system in their electrical and mechanical parts. This approach allows not only to adequately capture the complex dynamics behaviour of the TRMS but also the development of novel control algorithms based on nested feedback loops that offer a higher performance than classical control schemes. Moreover, the use of the Euler-Lagrange method in the modelling of the mechanical structure of the TRMS allows a higher adjustment with the real control laboratory platform in comparison with other analytical methods based on the Newtonian approach [25]. The dynamic modelling has been developed in two stages and validated by our research group by means of experimental identification trials. It is presented in the following subsections. The first subsection illustrates the dynamic model of the electrical part, and the second depicts the dynamic model of the mechanical part of the system.

2.1.1. Dynamics of the electrical part

The electrical part of the system is formed by the interface circuit and the DC motors of the main and tail rotors. The interface circuit is the internal electrical circuit that adapts the input control voltages, applied in MATLAB®/Simulink® (u_m for the main rotor and u_t for the tail rotor), to the actual voltage value of the DC motors (v_m for the main rotor and v_t for the tail

http://dx.doi.org/10.5772/64875

rotor). This interface can be modelled as a linear relationship [13], obtaining the following result:

$$v_m = k_{u_m} u_m \tag{1}$$

$$v_t = k_{u_t} u_t \tag{2}$$

where k_{u_m} and k_{u_t} denote the constant gains for the main and tail rotors, respectively. With regard to the DC motors, there are two identical permanent magnet motors, one in each rotor of the TRMS, with the only difference of the mechanical loads (the propellers). Bearing in mind that the dynamics of the motor´s current can be neglected [13], the DC motor dynamics for the main rotor and the tail rotor are the following ones:

$$v_m = R_m i_m + k_{v_m} \omega_m \tag{3}$$

$$v_t = R_t i_t + k_{v_t} \omega_t \tag{4}$$

where i_m and i_t are the motor currents (the subscripts m and t mean "main" and "tail"), R_m and R_t represent the motor resistances, and $k_{v_m} \omega_m$ and $k_{v_t} \omega_t$ denote the electromotive forces of each motor (ω_m and ω_t represent the angular velocities of the each motor). On the other hand, the electromechanical balance of the torques acting on each motor is expressed as:

$$I_{m_1} \dot{\omega}_m = k_{t_m} i_m - f_{v_m} \omega_m - C_{Q_m} \omega_m |\omega_m| \tag{5}$$

$$I_{t_1} \dot{\omega}_t = k_{t_t} i_t - f_{v_t} \omega_t - C_{Q_t} \omega_t |\omega_t| \tag{6}$$

being I_{m_1} and I_{t_1} are the moment of the inertia rotors, $k_{t_m} i_m$ and $k_{t_t} i_t$ denote the electromechanical torques generated by the DC motors, $f_{v_m} \omega_m$ and $f_{v_t} \omega_t$ are the friction torques and $C_{Q_m} \omega_m |\omega_m|$ and $C_{Q_t} \omega_t |\omega_t|$ illustrate the aerodynamic torques.

After substituting the expression for the current intensity of the respective motors [obtained from Eqs. (3) and (4)] and the linear relationships for the interface circuit Eqs. (1) and (2), in

Eqs. (5) and (6), and after operating and rearranging terms, the following two equations are yielded for the main and tail rotors of the TRMS:

$$I_{m_1}\dot{\omega}_m = \frac{k_{t_m}}{R_m}k_{u_m}u_m - \left(\frac{k_{t_m}k_{v_m}}{R_m} + f_{v_m}\right)\omega_m - C_{Q_m}\omega_m\left|\omega_m\right| \tag{7}$$

$$I_{t_1}\dot{\omega}_t = \frac{k_{t_t}}{R_t}k_{u_t}u_t - \left(\frac{k_{t_t}k_{v_t}}{R_t} + f_{v_t}\right)\omega_t - C_{Q_t}\omega_t\left|\omega_t\right| \tag{8}$$

The dynamics of the electrical part of the TRMS is now expressed in a matrix form, using the following compact notation:

$$\dot{\boldsymbol{\omega}}(t) = \boldsymbol{N}\boldsymbol{u}(t) + \boldsymbol{\Gamma}\left(\boldsymbol{\omega}(t)\right) \tag{9}$$

where $\boldsymbol{\omega}(t) = \left[\omega_m, \omega_t\right]^T$ and $\boldsymbol{u}(t) = \left[u_m, u_t\right]^T$ represent the vector of angular velocities and the input control voltages, respectively, and, $\boldsymbol{N}= diag(n_m,\ \ n_t)$ and $\boldsymbol{\Gamma}(\boldsymbol{\omega}(t)) = \left[\Gamma_m, \Gamma_t\right]^T$ are defined by:

$$\boldsymbol{N} = \begin{bmatrix} n_m & 0 \\ 0 & n_t \end{bmatrix} = \begin{bmatrix} \dfrac{k_{t_m}k_{u_m}}{I_{m_1}R_m} & 0 \\ 0 & \dfrac{k_{t_t}k_{u_t}}{I_{t_1}R_t} \end{bmatrix} \tag{10}$$

$$\boldsymbol{\Gamma}\left(\boldsymbol{\omega}(t)\right) = \begin{bmatrix} \Gamma_m \\ \Gamma_t \end{bmatrix} = \begin{bmatrix} -\left(\dfrac{k_{t_m}k_{v_m}}{R_m} + f_{v_m}\right)\dfrac{\omega_m}{I_{m_1}} - \dfrac{C_{Q_m}}{I_{m_1}}\omega_m\left|\omega_m\right| \\ -\left(\dfrac{k_{t_t}k_{v_t}}{R_t} + f_{v_t}\right)\dfrac{\omega_t}{I_{t_1}} - \dfrac{C_{Q_t}}{I_{t_1}}\omega_t\left|\omega_t\right| \end{bmatrix} \tag{11}$$

Finally, in order to complete the dynamic model of the electrical part of the TRMS, **Tables 1** and **2** show the parameters used in the model, indicating the description of the parameters, their values and their corresponding units. These values, which are based on the data presented in [13], have been experimentally tuned and validated in the dynamics identification tests that we have performed during our research.

http://dx.doi.org/10.5772/64875

Symbol	Parameter	Value	Units
k_{v_m}	Motor velocity constant	0.0202	$\mathrm{V\ rad^{-1}\ s}$
R_m	Motor armature resistance	8	Ω
L_m	Motor armature inductance	0.86×10^{-3}	H
k_{t_m}	Electromagnetic constant torque motor	0.0202	$\mathrm{N\ m\ \ A^{-1}}$
k_{u_m}	Coefficient linear relationship interface circuit	8.5	–
$C^{+}_{Q_m}$	Load factor ($\omega_m \geq 0$)	2.695×10^{-7}	$\mathrm{N\ m\ s^2\ rad^{-2}}$
$C^{-}_{Q_m}$	Load factor ($\omega_m < 0$)	2.46×10^{-7}	$\mathrm{N\ m\ s^2\ rad^{-2}}$
f_{v_m}	Viscous friction coefficient	3.89×10^{-6}	$\mathrm{N\ m\ rad^{-1}\ s}$
I_{m_1}	Moment of inertia about the axis of rotation	1.05×10^{-4}	$\mathrm{kg\ m^2}$

Table 1. Parameters of the main rotor.

Symbol	Parameter	Value	Units
k_{v_t}	Motor velocity constant	0.0202	$\mathrm{V\ rad^{-1}\ s}$
R_t	Motor armature resistance	8	Ω
L_t	Motor armature inductance	0.86×10^{-3}	H
k_{t_t}	Electromagnetic constant torque motor	0.0202	$\mathrm{N\ m\ A^{-1}}$
k_{u_t}	Coefficient linear relationship interface circuit	6.5	–
C_{Q_t}	Load factor	1.164×10^{-8}	$\mathrm{N\ m\ s^2\ rad^{-2}}$
f_{v_t}	Viscous friction coefficient	1.715×10^{-6}	$\mathrm{N\ m\ rad^{-1}\ s}$
I_{t_1}	Moment of inertia about the axis of rotation	2.1×10^{-5}	$\mathrm{kg\ m^2}$

Table 2. Parameters of the tail rotor.

2.1.2. Dynamics of the mechanical part

In the development of the dynamic model of the mechanical part, we consider the mechanics of the TRMS as an assembly of the following three components explained next. The first component is formed by the two rotors, their shields and the free-free beam that links together both rotors. The second component consists in the counterbalance and counterweight beam,

and finally, the third component is the pivoted beam. **Figure 2** helps to clarify the different components considered in the dynamics of the mechanical part of the system. From the previous division, and bearing in mind the notation used in **Figures 3** and **4**, the development of the dynamic model is achieved by means of the application of the Euler-Lagrange formulation. It can be summarised in the following steps:

1. Resolution of the forward kinematics of the three subsystems.
2. Evaluation of the kinetic energy.
3. Evaluation of the potential energy.
4. Obtaining the equations of motion.

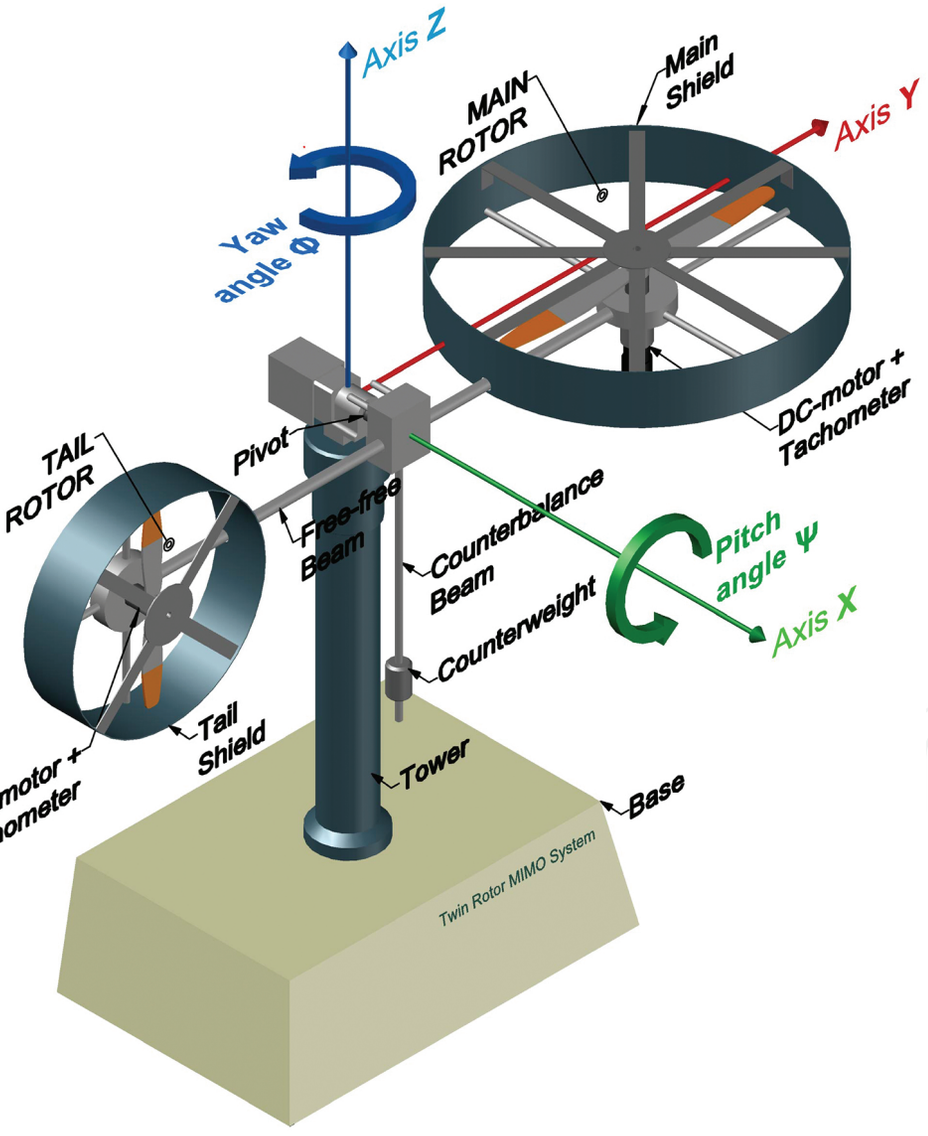

Figure 2. Twin rotor MIMO system (TRMS) prototype platform.

http://dx.doi.org/10.5772/64875

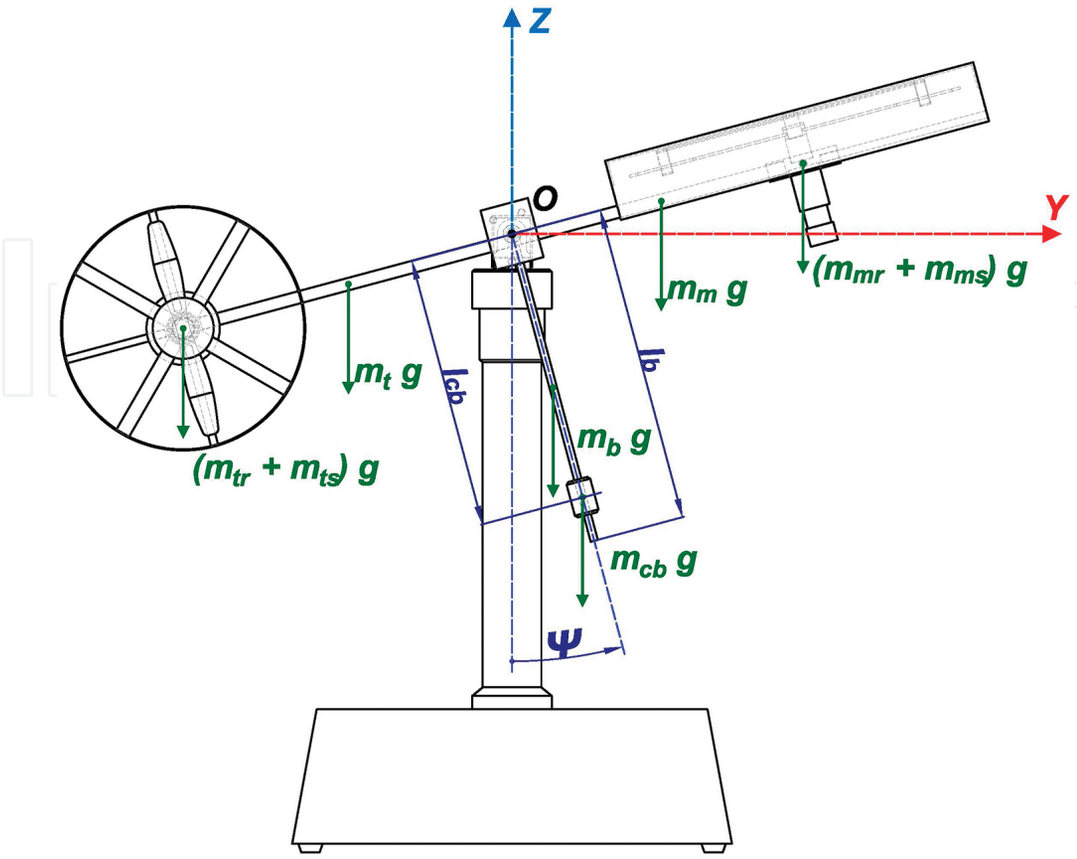

Figure 3. View of the TRMS on a vertical plane.

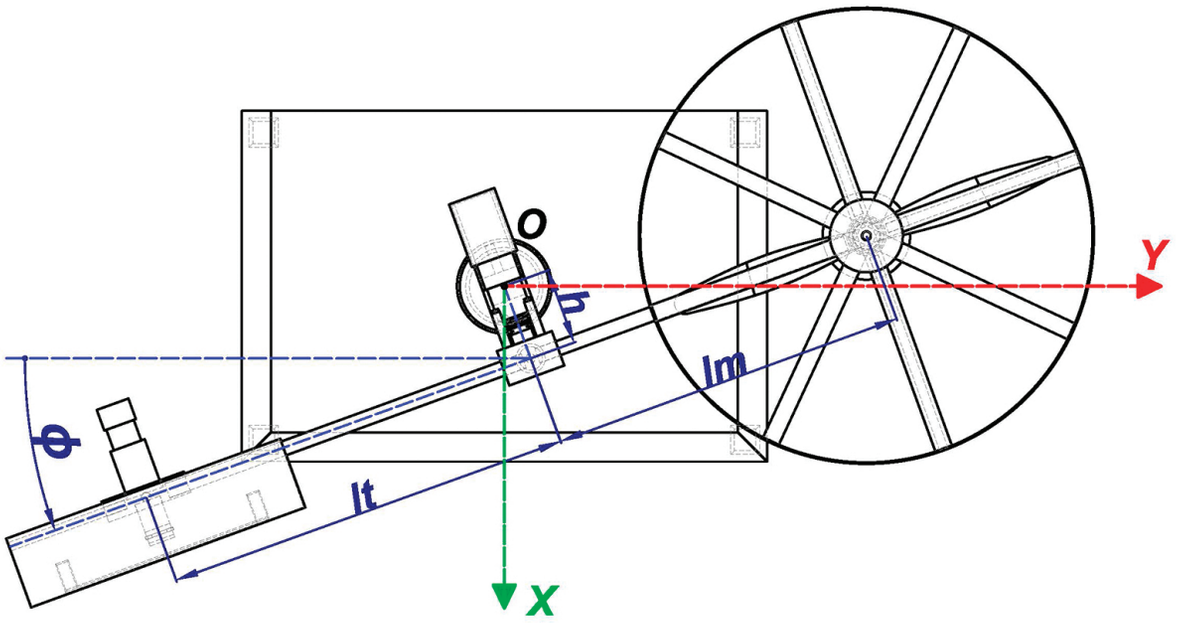

Figure 4. View of the TRMS on a horizontal plane.

2.1.2.1. Resolution of the forward kinematics of the system

The problem of direct kinematics of the TRMS consists in determining the spatial position of the three subsystems considered, according to the reference system located in the upper part of the platform (see **Figures 3** and **4**). Using the Denavit-Hartenberg method, we can express the position of a point on each subsystem (P_1, P_2, P_3) parameterised by R_1, R_2, R_3, which represents the distances between the considerate points and the reference system associated to each subsystem. The results of these positions are expressed in the following three equations (where: $S_\Psi \equiv \sin\Psi$, $C_\Psi \equiv \cos\Psi$, $S_\phi \equiv \sin\phi$ and $C_\phi \equiv \cos\phi$):

$$\boldsymbol{P}_1 = \begin{bmatrix} P_{1_x} & P_{1_y} & P_{1_z} \end{bmatrix}^T = \begin{bmatrix} -R_1 S_\phi C_\psi + hC_\phi & R_1 C_\phi C_\psi + hS_\phi & R_1 S_\psi \end{bmatrix}^T \tag{12}$$

$$\boldsymbol{P}_2 = \begin{bmatrix} P_{2_x} & P_{2_y} & P_{2_z} \end{bmatrix}^T = \begin{bmatrix} -R_2 S_\phi S_\psi + hC_\phi & R_2 C_\phi S_\psi + hS_\phi & -R_2 C_\psi \end{bmatrix}^T \tag{13}$$

$$\boldsymbol{P}_3 = \begin{bmatrix} P_{3_x} & P_{3_y} & P_{3_z} \end{bmatrix}^T = \begin{bmatrix} R_3 C_\phi & R_3 S_\phi & 0 \end{bmatrix}^T \tag{14}$$

2.1.2.2. Evaluation of the kinetic energy

In order to carry out the evaluation of the total kinetic energy of the TRMS, it is necessary to calculate the kinetic energy corresponding to each of the three subsystems previously defined. Starting with the first subsystem, its kinetic energy, T_1, yields:

$$T_1 = \frac{1}{2}\int |v_1|^2 \, dm(R_1) = \frac{1}{2} J_1 \left(C_\psi{}^2 \dot{\phi}^2 + \dot{\psi}^2 \right) + \frac{1}{2} h^2 m_{T_1} \dot{\phi}^2 - h S_\psi l_{T_1} m_{T_1} \dot{\phi}\dot{\psi} \tag{15}$$

$$|v_1|^2 = \left(R_1{}^2 C_\psi{}^2 + h^2 \right) \dot{\phi}^2 + R_1{}^2 \dot{\psi}^2 - 2 R_1 h S_\psi \dot{\phi}\dot{\psi} \tag{16}$$

where ψ and ϕ represent the yaw and the pitch angle, respectively, and m_{T_1}, l_{T_1}, and J_1 are obtained from the following expressions:

$$\int dm(R_1) = m_{\mathrm{m}} + m_{\mathrm{mr}} + m_{\mathrm{ms}} + m_{\mathrm{t}} + m_{\mathrm{tr}} + m_{\mathrm{ts}} = m_{T_1} \tag{17}$$

$$l_{T_1} = \frac{\int R_1 dm(R_1)}{\int dm(R_1)} = \frac{\left(\frac{m_{\mathrm{t}}}{2} + m_{\mathrm{tr}} + m_{\mathrm{ts}} \right) l_t - \left(\frac{m_{\mathrm{m}}}{2} + m_{\mathrm{mr}} + m_{\mathrm{ms}} \right) l_m}{m_{T_1}} \tag{18}$$

$$J_1 = \left(\frac{1}{3} m_{\mathrm{t}} + m_{\mathrm{tr}} + m_{\mathrm{ts}} \right) l_t{}^2 + \left(\frac{1}{3} m_{\mathrm{m}} + m_{\mathrm{mr}} + m_{\mathrm{ms}} \right) l_m{}^2 + m_{\mathrm{ts}} r_{\mathrm{ts}}{}^2 + \frac{1}{2} m_{\mathrm{ms}} r_{\mathrm{ms}}{}^2 \tag{19}$$

http://dx.doi.org/10.5772/64875

On the other hand, the kinetic energy for the second subsystem, T_2, results in:

$$T_2 = \frac{1}{2}\int |v_2|^2 \, dm(R_2) = \frac{1}{2} J_2 \left({S_\psi}^2 \dot{\phi}^2 + \dot{\psi}^2 \right) + \frac{1}{2} h^2 m_{T_2} \dot{\phi}^2 + h C_\psi l_{T_2} m_{T_2} \dot{\phi}\dot{\psi} \tag{20}$$

$$|v_2|^2 = \left({R_2}^2 {S_\psi}^2 + h^2 \right) \dot{\phi}^2 + {R_2}^2 \dot{\psi}^2 + 2 R_2 h C_\psi \dot{\phi}\dot{\psi} \tag{21}$$

in which the terms m_{T_2}, l_{T_2} and J_2 are the following:

$$\int dm(R_2) = m_{\mathrm{b}} + m_{\mathrm{cb}} = m_{T_2} \tag{22}$$

$$l_{T_2} = \frac{\int R_2 dm(R_2)}{\int dm(R_2)} = \frac{m_{\mathrm{b}} \dfrac{l_b}{2} + m_{\mathrm{cb}} l_{mcb}}{m_{T_2}} \tag{23}$$

$$J_2 = \frac{1}{3} m_{\mathrm{b}} {l_b}^2 + m_{\mathrm{cb}} {l_{cb}}^2 \tag{24}$$

On the other hand, the kinetic energy for the third subsystem, T_3, gives the following result:

$$T_3 = \frac{1}{2}\int |v_3|^2 \, dm(R_3) = \frac{1}{2} J_3 \dot{\phi}^2 \tag{25}$$

$$|v_3|^2 = {R_3}^2 \dot{\phi}^2 \tag{26}$$

being $J_3 = \frac{1}{3} m_h {l_h}^2$.

Finally, the total kinetic energy of the TRMS, T, is obtained as the sum of the kinetic energy of each subsystem (Eqs. (15), (20) and (25)). One obtains the following result:

$$\begin{aligned} T = T_1 + T_2 + T_3 = {} & \frac{1}{2}\left(J_1 {C_\psi}^2 + J_2 {S_\psi}^2 + J_3 + h^2 \left(m_{T_1} + m_{T_2} \right) \right) \dot{\phi}^2 \\ & + \frac{1}{2}\left(J_1 + J_2 \right) \dot{\psi}^2 + h \left(l_{T_2} m_{T_2} C_\psi - l_{T_1} m_{T_1} S_\psi \right) \dot{\phi}\dot{\psi} \end{aligned} \tag{27}$$

2.1.2.3. Evaluation of the potential energy

Following a similar procedure to the one used in the computation of the kinetic energy, the total potential energy of the TRMS, V, consists of the sum of the potential energy of each of the three subsystems, the free-free beam (including rotors and shields), the counterbalance beam and the pivoted beam. The following result is obtained:

$$V = V_1 + V_2 + V_3 = g\left(S_\psi l_{T_1} m_{T_1} - C_\psi l_{T_2} m_{T_2}\right) \tag{28}$$

where:

$$V_1 = g\int r_{z_1}\left(R_1\right) dm\left(R_1\right) = g\int P_{1_z}\, dm\left(R_1\right) = gS_\psi l_{T_1} m_{T_1} \tag{29}$$

$$V_2 = g\int r_{z_2}\left(R_2\right) dm\left(R_2\right) = g\int P_{2_z}\, dm\left(R_2\right) = -gC_\psi l_{T_2} m_{T_2} \tag{30}$$

$$V_3 = g\int r_{z_3}\left(R_3\right) dm\left(R_3\right) = g\int P_{3_z}\, dm\left(R_3\right) = 0 \tag{31}$$

2.1.2.4. Equations of motion of the TRMS

The last step in the mechanical dynamic model of the TRMS is obtaining the equations of motion of the system. The first step is the computation of the Lagrangian of the system, defined as the difference between the total kinetic energy, defined in Eq. (27), and the total potential energy, defined in Eq. (28), yielding the following:

$$\begin{aligned} L = T - V = {} & \frac{1}{2}\left(J_1 {C_\psi}^2 + J_2 {S_\psi}^2 + J_3 + h^2\left(m_{T_1} + m_{T_2}\right)\right)\dot{\phi}^2 \\ & + \frac{1}{2}\left(J_1 + J_2\right)\dot{\psi}^2 + h\left(l_{T_2} m_{T_2} C_\psi - l_{T_1} m_{T_1} S_\psi\right)\dot{\phi}\dot{\psi} - g\left(S_\psi l_{T_1} m_{T_1} - C_\psi l_{T_2} m_{T_2}\right) \end{aligned} \tag{32}$$

Once the Lagrangian function has been obtained, the equations of motion of the TRMS can be derived using Lagrange's formulation:

$$\frac{d}{dt}\left(\frac{\partial L}{\partial \dot{\psi}}\right) - \frac{\partial L}{\partial \psi} = \sum M_{iv} \tag{33}$$

http://dx.doi.org/10.5772/64875

$$\frac{d}{dt}\left(\frac{\partial L}{\partial \dot{\phi}}\right)-\frac{\partial L}{\partial \phi}=\sum M_{ih} \tag{34}$$

where $\sum \boldsymbol{M_{iv}}$ and $\sum \boldsymbol{M_{ih}}$ represent the sum of the torques of the external forces along the vertical and horizontal axes, respectively. The following expressions illustrate several partial results necessary to achieve the equations of motion represented by Eqs. (33) and (34):

$$\frac{\partial L}{\partial \dot{\psi}}=\left(J_1+J_2\right)\dot{\psi}+h\left(l_{T_2}m_{T_2}C_{\psi}-l_{T_1}m_{T_1}S_{\psi}\right)\dot{\phi} \tag{35}$$

$$\frac{\partial L}{\partial \psi}=\left(\left(J_2-J_1\right)C_{\psi}S_{\psi}\right)\dot{\phi}^2-h\left(l_{T_1}m_{T_1}C_{\psi}+l_{T_2}m_{T_2}S_{\psi}\right)\dot{\phi}\dot{\psi}-g\left(l_{T_1}m_{T_1}C_{\psi}+l_{T_2}m_{T_2}S_{\psi}\right) \tag{36}$$

$$\frac{\partial L}{\partial \dot{\phi}}=\left(J_1{C_{\psi}}^2+J_2{S_{\psi}}^2+J_3+h^2\left(m_{T_1}+m_{T_2}\right)\right)\dot{\phi}+h\left(l_{T_2}m_{T_2}C_{\psi}-l_{T_1}m_{T_1}S_{\psi}\right)\dot{\psi} \tag{37}$$

$$\frac{\partial L}{\partial \phi}=0 \tag{38}$$

$$\frac{d}{dt}\left(\frac{\partial L}{\partial \dot{\psi}}\right)=h\left(l_{T_2}m_{T_2}C_{\psi}-l_{T_1}m_{T_1}S_{\psi}\right)\ddot{\phi}+\left(J_1+J_2\right)\ddot{\psi}-h\left(l_{T_1}m_{T_1}C_{\psi}+l_{T_2}m_{T_2}S_{\psi}\right)\dot{\phi}\dot{\psi} \tag{39}$$

$$\begin{aligned}\frac{d}{dt}\left(\frac{\partial L}{\partial \dot{\phi}}\right)=&\left(J_1{C_{\psi}}^2+J_2{S_{\psi}}^2+J_3+h^2\left(m_{T_1}+m_{T_2}\right)\right)\ddot{\phi}-h\left(l_{T_1}m_{T_1}S_{\psi}-l_{T_2}m_{T_2}C_{\psi}\right)\ddot{\psi}\\&-h\left(l_{T_1}m_{T_1}C_{\psi}+l_{T_2}m_{T_2}S_{\psi}\right)\dot{\psi}^2+2\left(\left(J_2-J_1\right)C_{\psi}S_{\psi}\right)\dot{\phi}\dot{\psi}\end{aligned} \tag{40}$$

The sum of the external torques in the vertical axis is shown next:

$$\begin{aligned}\sum M_{iv}&=M_{T_m}-M_{R_t}-M_{F_{\psi}}+M_{I_t}\\\sum M_{iv}&=C_{T_m}\omega_m\left|\omega_m\right|l_m-C_{R_t}\omega_t\left|\omega_t\right|-\left(f_{v_{\psi}}\dot{\psi}+f_{c_{\psi}}sgn\left(\dot{\psi}\right)\right)+k_t\dot{\omega}_t\end{aligned} \tag{41}$$

where $M_{T_m}=C_{T_m}\omega_m\left|\omega_m\right|l_m$ expresses the aerodynamic thrust torque caused by the rotation of the main propeller, $M_{R_t}=C_{R_t}\omega_t\left|\omega_t\right|$ denotes the load torque created by air resistance in the tail rotor, $M_{F_{\psi}}=\left(f_{v_{\psi}}\dot{\psi}+f_{c_{\psi}}sgn\left(\dot{\psi}\right)\right)$ represents the load torque as a result of the friction (including the viscous effects and the Coulomb friction), and $M_{I_t}=k_t\dot{\omega}_t$ represents the inertial counter torque that is caused by the reaction produced by a change in the rotational speed of the tail rotor.

On the other hand, the sum of the external torques in the horizontal axis is as follows:

$$\begin{aligned}\sum M_{ih} &= M_{T_t} - M_{R_m} - M_{F_\phi} - M_c + M_{I_m} \\ \sum M_{ih} &= C_{T_T}\omega_t|\omega_t|l_t C_\psi - C_{R_m}\omega_m|\omega_m|C_\psi \\ &\quad -\left(f_{v_\phi}\dot{\phi} + f_{c_\phi} sgn\left(\dot{\phi}\right)\right) - C_c\left(\phi - \phi_0\right) + k_m\dot{\omega}_m C_\psi\end{aligned} \tag{42}$$

where $M_{T_t} = C_{T_T}\omega_t|\omega_t|l_t C_\psi$ expresses the aerodynamic thrust torque of the tail propeller, $M_{R_m} = C_{R_m}\omega_m|\omega_m|C_\psi$ represents the load torque created by air resistance in the main rotor, $M_{F_\phi} = (f_{v_\phi}\dot{\phi} + f_{c_\phi} sgn(\dot{\phi}))$ denotes the load torque as a result of the friction (including the viscous effects and the Coulomb friction), $M_c = C_c(\phi - \phi_0)$ is the magnitude of torque exerted by the cable (it has a certain stiffness that allows to model it as a spring)), and finally $M_{I_m} = k_m\dot{\omega}_m C_\psi$ represents the inertial counter torque that is caused by the reaction produced by a change in the rotational speed of the main rotor.

Upon merging Eq. (33) to Eq. (42), and after performing some rearrangements, one obtains the following result for the equations of motion:

$$\begin{aligned}&\left(J_1 + J_2\right)\ddot{\psi} + h\left(l_{T_2} m_{T_2} C_\psi - l_{T_1} m_{T_1} S_\psi\right)\ddot{\phi} + \left(\frac{\left(J_1 - J_2\right)}{2} S_{2\psi}\right)\dot{\phi}^2 + g\left(l_{T_1} m_{T_1} C_\psi + l_{T_2} m_{T_2} S_\psi\right) \\ &= C_{T_m}\omega_m|\omega_m|l_m - C_{R_t}\omega_t|\omega_t| - \left(f_{v_\psi}\dot{\psi} + f_{c_\psi} sgn\left(\dot{\psi}\right)\right) + k_t\dot{\omega}_t\end{aligned} \tag{43}$$

$$\begin{aligned}&h\left(l_{T_2} m_{T_2} C_\psi - l_{T_1} m_{T_1} S_\psi\right)\ddot{\psi} + \left(J_1 C_\psi{}^2 + J_2 S_\psi{}^2 + J_3 + h^2\left(m_{T_1} + m_{T_2}\right)\right)\ddot{\phi} - \\ &h\left(l_{T_1} m_{T_1} C_\psi + l_{T_2} m_{T_2} S_\psi\right)\dot{\psi}^2 + \left(\left(J_2 - J_1\right) S_{2\psi}\right)\dot{\phi}\dot{\psi} \\ &= C_{T_T}\omega_t|\omega_t|l_t C_\psi - C_{R_m}\omega_m|\omega_m|C_\psi - \left(f_{v_\phi}\dot{\phi} + f_{c_\phi} sgn\left(\dot{\phi}\right)\right) - C_c\left(\phi - \phi_0\right) + k_m\dot{\omega}_m C_\psi\end{aligned} \tag{44}$$

If we use matrix notation, the dynamic model of the mechanical part of the TRMS can be expressed in a compact form:

$$\boldsymbol{M}\left(\boldsymbol{q}(t)\right)\ddot{\boldsymbol{q}}(t) + \boldsymbol{C}\left(\boldsymbol{q}(t), \dot{\boldsymbol{q}}(t)\right)\dot{\boldsymbol{q}}(t) + \boldsymbol{\eta}(\boldsymbol{q}(t), \dot{\boldsymbol{q}}(t), \dot{\boldsymbol{\omega}}(t)) = \boldsymbol{E}\left(\boldsymbol{q}(t)\right)\boldsymbol{\Omega}(t) \tag{45}$$

in which $\boldsymbol{q}(t) = [\psi(t), \ \ \phi(t)]^T$ is the vector of generalised coordinates of the TRMS, $\boldsymbol{\omega}(t) = \left[\omega_m(t), \ \ \omega_t(t)\right]^T$ is the angular velocity vector, and the matrices $\boldsymbol{M}(\boldsymbol{q}(t))$, $\boldsymbol{C}(\boldsymbol{q}(t), \dot{\boldsymbol{q}}(t))$, $\boldsymbol{E}(\boldsymbol{q}(t))$, and the vectors $\boldsymbol{\Omega}(t)$ and $\boldsymbol{\eta}(\boldsymbol{q}(t), \dot{\boldsymbol{q}}(t), \dot{\boldsymbol{\omega}}(t))$ are given by:

http://dx.doi.org/10.5772/64875

$$\boldsymbol{M}\left(\boldsymbol{q}(t)\right)=\begin{bmatrix} J_1+J_2 & h\left(l_{T_2}m_{T_2}C_\psi - l_{T_1}m_{T_1}S_\psi\right) \\ h\left(l_{T_2}m_{T_2}C_\psi - l_{T_1}m_{T_1}S_\psi\right) & J_1{C_\psi}^2 + J_2{S_\psi}^2 + J_3 + h^2\left(m_{T_1}+m_{T_2}\right) \end{bmatrix} \tag{46}$$

$$\boldsymbol{C}\left(\boldsymbol{q}(t),\dot{\boldsymbol{q}}(t)\right)=\begin{bmatrix} 0 & \frac{1}{2}\left(J_1-J_2\right)S_{2\psi}\dot{\phi} \\ -h\left(l_{T_1}m_{T_1}C_\psi + l_{T_2}m_{T_2}S_\psi\right)\dot{\psi} & \left(J_2-J_1\right)S_{2\psi}\dot{\psi} \end{bmatrix} \tag{47}$$

$$\boldsymbol{E}\left(\boldsymbol{q}(t)\right)=\begin{bmatrix} C_{T_m}l_m & -C_{R_t} \\ -C_{R_m}C_\psi & C_{T_T}l_tC_\psi \end{bmatrix} \tag{48}$$

$$\boldsymbol{\Omega}(t)=\begin{bmatrix} \omega_m\left|\omega_m\right| \\ \omega_t\left|\omega_t\right| \end{bmatrix} \tag{49}$$

$$\boldsymbol{\eta}\left(\boldsymbol{q}(t),\dot{\boldsymbol{q}}(t),\dot{\boldsymbol{\omega}}(t)\right)=\boldsymbol{G}\left(\boldsymbol{q}(t)\right)+\boldsymbol{F}\left(\dot{\boldsymbol{q}}(t)\right)+\boldsymbol{T}\left(\boldsymbol{q}(t),\dot{\boldsymbol{\omega}}(t)\right) \tag{50}$$

$$\boldsymbol{G}\left(\boldsymbol{q}(t)\right)=\begin{bmatrix} g\left(l_{T_1}m_{T_1}C_\psi + l_{T_2}m_{T_2}S_\psi\right) \\ 0 \end{bmatrix} \tag{51}$$

$$\boldsymbol{F}\left(\dot{\boldsymbol{q}}(t)\right)=\boldsymbol{F_v}\dot{\boldsymbol{q}}(t)+\boldsymbol{F_c}\left(\dot{\boldsymbol{q}}(t)\right)=\begin{bmatrix} f_{v_\psi} & 0 \\ 0 & f_{v_\phi} \end{bmatrix}\dot{\boldsymbol{q}}(t)+\begin{bmatrix} f_{c_\psi}sgn\left(\dot{\psi}\right) \\ f_{c_\phi}sgn\left(\dot{\phi}\right) \end{bmatrix}=\begin{bmatrix} f_{v_\psi}\dot{\psi}+f_{c_\psi}sgn\left(\dot{\psi}\right) \\ f_{v_\phi}\dot{\phi}+f_{c_\phi}sgn\left(\dot{\phi}\right) \end{bmatrix} \tag{52}$$

$$\begin{aligned} \boldsymbol{T}\left(\boldsymbol{q}(t),\dot{\boldsymbol{\omega}}(t)\right) &= \boldsymbol{M_c}\left(\boldsymbol{q}(t)\right)-\boldsymbol{M_g}\left(\boldsymbol{q}(t)\right)\dot{\boldsymbol{\omega}}(t)=\begin{bmatrix} 0 \\ C_c(\phi-\phi_0) \end{bmatrix}-\begin{bmatrix} 0 & k_t \\ k_mC_\psi & 0 \end{bmatrix}\dot{\boldsymbol{\omega}}(t) \\ &= \begin{bmatrix} -k_t\dot{\omega}_t \\ C_c(\phi-\phi_0)-k_m\dot{\omega}_mC_\psi \end{bmatrix} \end{aligned} \tag{53}$$

Finally, after substituting Eqs. (51)–(53) into Eq. (50), the following yields:

$$\boldsymbol{\eta}\left(\boldsymbol{q}(t),\dot{\boldsymbol{q}}(t),\dot{\boldsymbol{\omega}}(t)\right)=\begin{bmatrix} g\left(l_{T_1}m_{T_1}C_\psi + l_{T_2}m_{T_2}S_\psi\right)+f_{v_\psi}\dot{\psi}+f_{c_\psi}sgn\left(\dot{\psi}\right)-k_t\dot{\omega}_t \\ f_{v_\phi}\dot{\phi}+f_{c_\phi}sgn\left(\dot{\phi}\right)+C_c\left(\phi-\phi_0\right)-k_m\dot{\omega}_mC_\psi \end{bmatrix} \tag{54}$$

Symbol	Parameter	Value	Units
l_{t}	Length of the tail part of the free-free beam	0.282	m
l_{m}	Length of the main part of the free-free beam	0.246	m
l_{b}	Length of the counterbalance beam	0.290	m
l_{cb}	Distance between the counterweight and the join	0.276	m
r_{ms}	Radius of the main shield	0.155	m
r_{ts}	Radius of the tail shield	0.1	m
h	Length of the pivoted beam	0.06	m
m_{tr}	Mass of the tail DC motor and tail rotor	0.221	kg
m_{mr}	Mass of the main DC motor and main rotor	0.236	kg
m_{cb}	Mass of the counterweight	0.068	kg
m_{t}	Mass of the tail part of the free-free beam	0.015	kg
m_{m}	Mass of the main part of the free-free beam	0.014	kg
m_{b}	Mass of the counterbalance beam	0.022	kg
m_{ts}	Mass of the tail shield	0.119	kg
m_{ms}	Mass of the main shield	0.219	kg
m_{h}	Mass of pivoted beam	0.01	kg

Table 3. Mechanical parameters.

Symbol	Parameter	Value	Units
$C_{T_m}^{+}$	Thrust torque coefficient of the main rotor ($\omega_m \geq 0$)	1.53×10^{-5}	$\mathrm{N\,s^2\,rad^{-2}}$
$C_{T_m}^{-}$	Thrust torque coefficient of the main rotor ($\omega_m < 0$)	8.8×10^{-6}	$\mathrm{N\,s^2\,rad^{-2}}$
C_{R_t}	Load torque coefficient of the tail rotor	9.7×10^{-8}	$\mathrm{N\,m\,s^2\,rad^{-2}}$
f_{v_ψ}	Viscous friction coefficient	0.0024	$\mathrm{N\,m\,s\,rad^{-1}}$
f_{c_ψ}	Coulomb friction coefficient	5.69×10^{-4}	N m
k_{t}	Coefficient of the inertial counter torque created by the change in ω_t	2.6×10^{-5}	$\mathrm{N\,m\,s^2\,rad^{-1}}$

Table 4. Parameters of the pitch movement.

Symbol	Parameter	Value	Units
$C_{T_t}^{+}$	Thrust torque coefficient of the tail rotor ($\omega_t \geq 0$)	3.25×10^{-6}	$\mathrm{N\,s^2\,rad^{-1}}$
$C_{T_t}^{-}$	Thrust torque coefficient of the tail rotor ($\omega_t < 0$)	1.72×10^{-6}	$\mathrm{N\,s^2\,rad^{-2}}$
$C_{R_m}^{+}$	Load torque coefficient of the main rotor ($\omega_m \geq 0$)	4.9×10^{-7}	$\mathrm{N\,m\,s^2\,rad^{-2}}$
$C_{R_m}^{-}$	Load torque coefficient of the main rotor ($\omega_m < 0$)	4.1×10^{-7}	$\mathrm{N\,m\,s^2\,rad^{-2}}$
f_{v_ϕ}	Viscous friction coefficient	0.03	$\mathrm{N\,m\,s\,rad^{-1}}$
f_{c_ϕ}	Coulomb friction coefficient	3×10^{-4}	N m
C_c	Coefficient of the elastic force torque created by the cable	0.016	$\mathrm{N\,m\,rad^{-1}}$
ϕ_0	Constant for the calculation of the torque of the cable	0	rad
k_m	Coefficient of the inertial counter torque created by the change in ω_m	2×10^{-4}	$\mathrm{N\,m\,s^2\,rad^{-1}}$

Table 5. Parameters of the yaw movement.

Finally, in order to complete the dynamic modelling for the mechanical part of the TRMS, **Tables 3–5** show in detail the parameters used in the model. For each parameter, its description, its value and the corresponding units is included. The initial approximation of these values was based in the developments described in [13]. Additionally, some values of the parameters have been tuned by carrying out several identification trials.

3. Design of the control system

In this section, the proposed nonlinear control for the TRMS platform is described. The proposed control is based on the division between the electrical and mechanical dynamics of the system and uses a cascade-type nonlinear control algorithm. **Figure 5** displays the proposed control scheme. As it can be observed, the proposed design is composed of two independent stages (or control loops) that are utilised to achieve stabilisation and precise trajectory tracking tasks for the controlled position of the generalised system coordinates. It should be noted that the proposed solution has been designed to overcome one of the limitations of the TRMS, which is the fact of being an underactuated system. As result of this fact, it only has two control actions (the input voltages of the main and tail rotors) to control the four degrees of freedom of the system (the pitch and yaw angles, and the angular velocities of the propellers). In this way, in order to meet this objective, once the dynamics of the TRMS have been decoupled, a nonlinear multivariable inner loop is closed to control the vector of the

angular velocities, and then, a nonlinear multivariable outer loop is closed to control the vector of the generalised coordinates of the system. This solution, based on a control scheme with two nested loops, allows a simplification in the design procedure as a result of its division into two simpler processes. Moreover, the scheme can be implemented more easily and safely than the standard controllers.

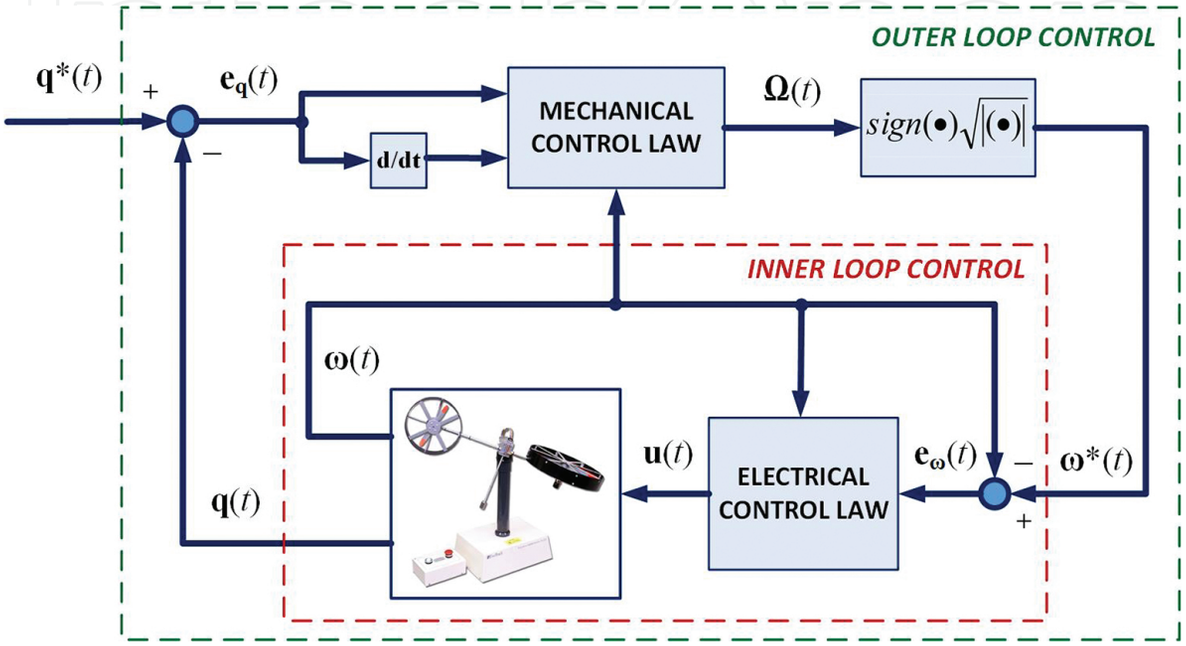

Figure 5. Nonlinear control scheme for the TRMS.

In the following subsections we describe the specifications and objectives of each control loop, defined as the inner loop or electrical controller and the outer loop or mechanical controller.

3.1. Inner loop control

The objective of the inner loop control is to determine the input voltages of the main and tail rotors (simulated in the MATLAB®/Simulink® environment), $\boldsymbol{u}(t) = \left[u_m, u_t\right]^T$, in order to eliminate the difference between the vector of reference angular velocities, $\boldsymbol{\omega}^*(t) = \left[\omega_m^*, \omega_t^*\right]^T$, calculated in the outer loop stage (as will be described in the next subsection), and the current vector of angular velocities of the propellers of the TRMS, $\boldsymbol{\omega}(t) = \left[\omega_m, \omega_t\right]^T$.

The magnitude of the input control voltage vector, $\boldsymbol{u}(t)$, necessary to achieve an asymptotically stable convergent behaviour of the tracking error trajectories, is calculated as the following nonlinear control law:

$$\boldsymbol{u}(t) = \boldsymbol{N}^{-1}\left[\boldsymbol{\gamma}_e(t) - \boldsymbol{\Gamma}(\boldsymbol{\omega}(t))\right] \tag{55}$$

http://dx.doi.org/10.5772/64875

where $\boldsymbol{N}$ and $\boldsymbol{\Gamma}(\boldsymbol{\omega}(t))$ where defined in Eqs. (10) and (11), respectively, and $\boldsymbol{\gamma_e}(t) = \left[\gamma_m, \gamma_t\right]^T$ represents a vector of auxiliary control inputs, given by the following expression:

$$\boldsymbol{\gamma}_e(t) = -\boldsymbol{K_P^e}\boldsymbol{e}_{\boldsymbol{\omega}}(t) = -\boldsymbol{K_P^e}[\boldsymbol{\omega}(t) - \boldsymbol{\omega}^*(t)] \tag{56}$$

where $\boldsymbol{K_P^e} \in \mathbb{R}^{2\times 2}$ is a constant diagonal positive definite matrix that represents the design elements of a vector-valued classical proportional controller and $\boldsymbol{e_\omega}(t) = \boldsymbol{\omega}(t) - \boldsymbol{\omega}^*(t)$ is the angular velocity error vector, which satisfies the following predominantly linear dynamic:

$$\dot{\boldsymbol{\omega}}(t) + \boldsymbol{K_P^e}\boldsymbol{e}_{\boldsymbol{\omega}}(t) = \boldsymbol{0} \tag{57}$$

Finally, the coefficients of the matrix $\boldsymbol{K_P}^e$ are chosen so as to render the closed-loop characteristic polynomial vectors into a Hurwitz polynomial vector with desirable roots.

3.2. Outer loop control

The aim of the outer loop control (mechanical controller) is to determine the required values for the angular velocities of the two rotors, $\boldsymbol{\omega}^*(t) = \left[\omega_m^*, \omega_t^*\right]^T$, which will be the reference inputs of the electrical loop (described in the above subsection), in order to eliminate the difference between the generalised coordinates of the TRMS, $\boldsymbol{q}(t) = [\psi, \phi]^T$, and the reference trajectories for the generalised coordinates of the TRMS $\boldsymbol{q}^*(t) = [\psi^*, \phi^*]^T$.

As a previous step for determining the mechanical control law, a simplification in the dynamic mechanical modelling of the TRMS has been considered. If we assume that the movement of the platform is sufficiently smooth, the terms of the inertial counter torques, which are caused by the reaction produced by the changes in the rotational speed of each rotor, $M_{I_t} = k_t\dot{\omega}_t$ and $M_{I_m} = k_m\dot{\omega}_m C_\psi$ included in Eqs. (53) and (54), can be considered negligible in comparison with the other terms. In this way, the dynamic equation of the mechanical part of the TRMS can be rewritten as:

$$\boldsymbol{M}\left(\boldsymbol{q}(t)\right)\ddot{\boldsymbol{q}}(t) + \boldsymbol{D}\left(\boldsymbol{q}(t), \dot{\boldsymbol{q}}(t)\right) = \boldsymbol{E}\left(\boldsymbol{q}(t)\right)\boldsymbol{\Omega}(t) \tag{58}$$

where the matrices $\boldsymbol{M}(\boldsymbol{q}(t))$, $\boldsymbol{E}(\boldsymbol{q}(t))$, and $\boldsymbol{\Omega}(t)$ were defined in the previous section and the new matrix $\boldsymbol{D}(\boldsymbol{q}(t), \dot{\boldsymbol{q}}(t)) = \left[D_\psi, D_\phi\right]^T$ is given by:

$$D_\psi = \frac{1}{2}\left(J_1 - J_2\right)S_{2\psi}\dot{\phi}^2 + g\left(l_{T_1}m_{T_1}C_\psi + l_{T_2}m_{T_2}S_\psi\right) + \left(f_{v_\psi}\dot{\psi} + f_{c_\psi}sgn\left(\dot{\psi}\right)\right) \tag{59}$$

$$D_{\phi} = -h\left(l_{T_1} m_{T_1} C_{\psi} + l_{T_2} m_{T_2} S_{\psi}\right)\dot{\psi}^2 + \left(\left(J_2 - J_1\right) S_{2\psi}\right)\dot{\phi}\dot{\psi} + \left(f_{v_{\phi}}\dot{\phi} + f_{c_{\phi}} sgn\left(\dot{\phi}\right)\right) + C_c\left(\phi - \phi_0\right) \tag{60}$$

The following nonlinear feedback control input vector, $\boldsymbol{\Omega}(t)$, is synthesised as a multivariable proportional-derivative (PD) controller with a cancellation term:

$$\boldsymbol{\Omega}(t) = \boldsymbol{E}^{-1}\left(\boldsymbol{q}(t)\right)\left[\boldsymbol{M}\left(\boldsymbol{q}(t)\right)\boldsymbol{\gamma_m}(t) + \boldsymbol{D}\left(\boldsymbol{q}(t), \dot{\boldsymbol{q}}(t)\right)\right] \tag{61}$$

where $\boldsymbol{\gamma}_m(t) = \left[\gamma_{\psi}, \gamma_{\phi}\right]^T$ is given by the following expression:

$$\boldsymbol{\gamma_m}(t) = \ddot{\boldsymbol{q}}(t) = \ddot{\boldsymbol{q}}^*(t) - \boldsymbol{K_D^m}\left(\dot{\boldsymbol{q}}(t) - \dot{\boldsymbol{q}}^*(t)\right) - \boldsymbol{K_P^m}\left(\boldsymbol{q}(t) - \boldsymbol{q}^*(t)\right) \tag{62}$$

in which $\boldsymbol{K_D^m}$ and $\boldsymbol{K_P^m} \in \mathbb{R}^{2\times 2}$ are the diagonal positive definite matrices that represent the design elements of a vector-valued classical PD controller. Thereby, for the mechanical part, the closed loop tracking error vector, $\boldsymbol{e_q}(t) = \boldsymbol{q}(t) - \boldsymbol{q}^*(t)$, evolves governed by:

$$\ddot{\boldsymbol{e}}_{\boldsymbol{q}}(t) + \boldsymbol{K_D^m}\dot{\boldsymbol{e}}_{\boldsymbol{q}}(t) + \boldsymbol{K_P^m}\boldsymbol{e_q}(t) = 0 \tag{63}$$

The controller design matrices $\boldsymbol{K_D^m}$ and $\boldsymbol{K_P^m}$ have been selected based in the philosophy used for the electrical controller. They must be selected to render closed-loop characteristic polynomial vectors into a Hurwitz polynomial vector with desirable roots. Finally, the necessary angular velocity vector values, $\boldsymbol{\omega}^*(t) = \left[\omega_m^*, \omega_t^*\right]^T$, are obtained from the input control vector, $\boldsymbol{\Omega}(t) = \left[\omega_m|\omega_m| \;\; \omega_t|\omega_t|\right]^T$, by performing the following operation:

$$\boldsymbol{\omega}^*(t) = \begin{bmatrix} \omega_m^* \\ \omega_t^* \end{bmatrix} = \begin{bmatrix} sgn\left(\omega_m|\omega_m|\right)\cdot\sqrt{\left|\omega_m|\omega_m|\right|} \\ sgn\left(\omega_t|\omega_t|\right)\cdot\sqrt{\left|\omega_t|\omega_t|\right|} \end{bmatrix} \tag{64}$$

4. Results

This section describes the numerical simulations carried out in the MATLAB®/Simulink® environment for the sake of verifying the efficiency of the proposed control approach in terms of quick convergence of the tracking errors to a small neighbourhood of zero, smooth transient

http://dx.doi.org/10.5772/64875

responses and low control effort. In the simulations, the desired reference trajectory for the pitch (ψ) and the yaw (ϕ) angles have been defined by the next expression:

$$\boldsymbol{q}^{*}(t)=\begin{bmatrix}\psi^{*}\\ \phi^{*}\end{bmatrix}=\begin{bmatrix}A_{0_\psi}+A_{1_\psi}\left(2\sin\left(\omega_{1_\psi}t\right)+\sin\left(\omega_{2_\psi}t\right)\right)\\ A_{1_\phi}\sin\left(\omega_{1_\phi}t\right)+A_{2_\phi}\left(\sin\left(\omega_{2_\phi}t\right)+\sin\left(\omega_{3_\phi}t\right)\right)\end{bmatrix} \tag{65}$$

where $\boldsymbol{q}^{*}(t)=[\psi^{*}(t),\phi^{*}(t)]^{T}$ is the reference trajectory vector of the generalised coordinates, and the values of the constants used in the above expressions are given by:

$$A_{0_\psi}=0.4\text{ rad};\quad A_{1_\psi}=0.1\text{ rad};\quad A_{1_\phi}=0.8\text{ rad};\quad A_{2_\phi}=0.3\text{ rad}; \tag{66}$$

$$\omega_{1_\psi}=0.0785\text{ rad/s};\quad \omega_{2_\psi}=0.0157\text{ rad/s}; \tag{67}$$

$$\omega_{1_\phi}=0.157\text{ rad/s};\quad \omega_{2_\phi}=0.0785\text{ rad/s};\quad \omega_{3_\phi}=0.0157\text{ rad/s}; \tag{68}$$

On the other hand, the values used in the simulation of the dynamic model of the TRMS, electrical parameters (main and tail rotors), mechanical parameters and dimensional parameters of the platform are detailed in **Tables 1–5**. The initial position of the TRMS has been defined as $\boldsymbol{q}_0(t)=\left[\psi_0,\phi_0\right]^{T}=[0,0]^{T}$ rad, representing a different value of the initial position than the reference trajectory vector. This choice of the starting position has been made to demonstrate the exponential convergence of the desired trajectories. With regard to the controller design parameters, it must be remarked that they have been selected to make the dynamics of the inner loop much faster than the outer loop dynamics, all this in order to ensure the functioning of the cascade controller [26]. The resulting values are as follows:

$$\boldsymbol{K_P^e}=diag(10.5,6.2); \tag{69}$$

$$\boldsymbol{K_D^m}=diag\left(8.20,3.85\right);\quad \boldsymbol{K_P^m}=diag(13.20,2.205); \tag{70}$$

Figures 6 and **7** show the performance of the proposed control scheme. **Figure 6** illustrates a comparative between the desired trajectory, $\boldsymbol{q}^{*}(t)=[\psi^{*}(t),\phi^{*}(t)]^{T}$, and the real trajectory of the TRMS, $\boldsymbol{q}(t)=[\psi(t),\phi(t)]^{T}$. The difference between these trajectories, or, in other words, the error vector of generalised coordinates, $\boldsymbol{e_q}(t)=\boldsymbol{q}(t)-\boldsymbol{q}^{*}(t)=[\psi(t)-\psi^{*}(t),\phi(t)-\phi^{*}(t)]^{T}$, is represented in **Figure 7**. The exponential convergence of the desired trajectories is observed,

with the error bounded to a small neighbourhood to zero, and the robustness against large initial errors.

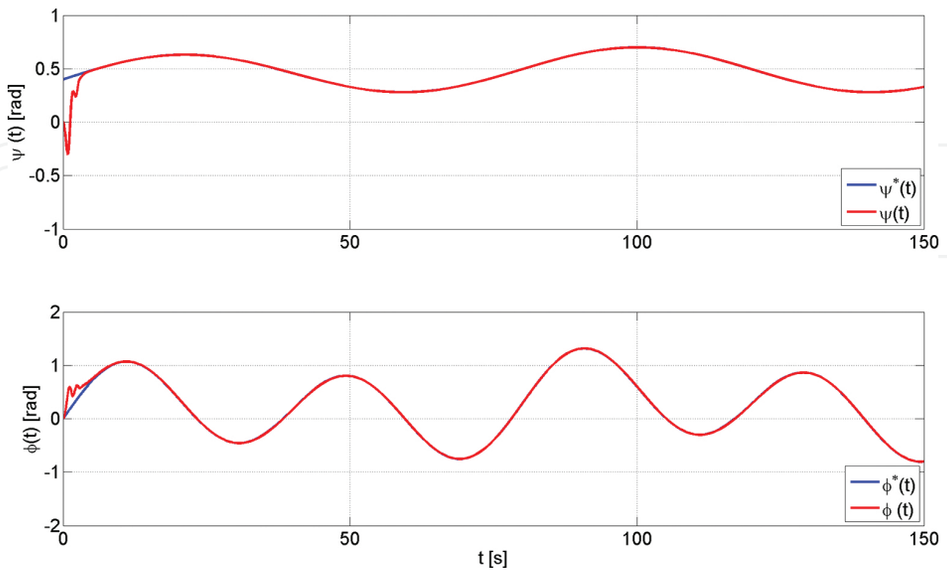

Figure 6. Real and desired evolution of the vector of generalised coordinates of the TRMS, $\boldsymbol{q}(t) = [\psi(t), \phi(t)]^T$.

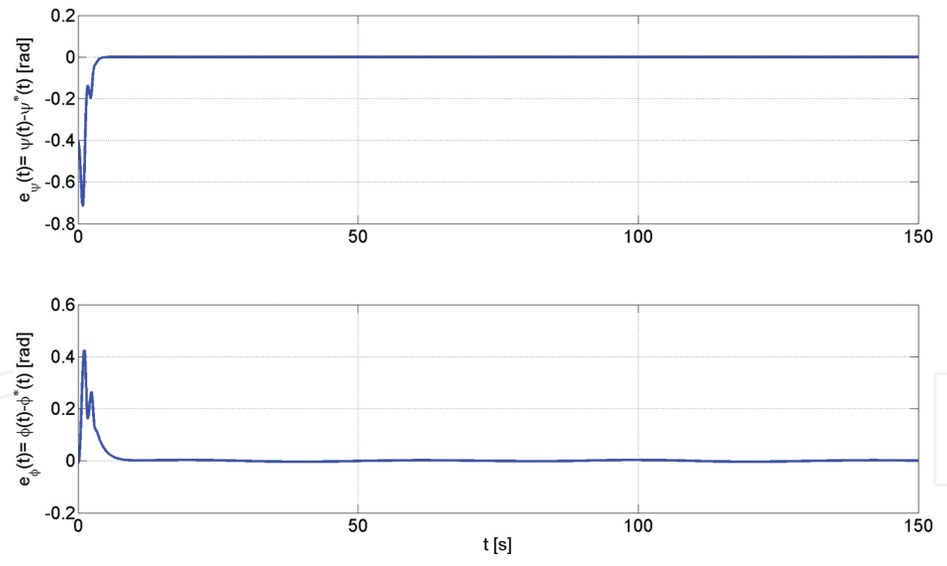

Figure 7. Evolution of the error vector of the generalised coordinates of the TRMS, $\boldsymbol{e_q}(t) = \boldsymbol{q}(t) - \boldsymbol{q}^*(t) = [\psi(t) - \psi^*(t), \phi(t) - \phi^*(t)]^T$.

Another graph that shows the excellent performance of the outer control loop is shown in **Figure 8**, where the auxiliary control input vector of the mechanical proportional-derivative (PD) controller (Eq. (62)) can be observed. This figure shows the quick convergence of the auxiliary control inputs of the mechanical controller to a small value of the origin in the

http://dx.doi.org/10.5772/64875

reference trajectory tracking vector error phase space, $\boldsymbol{e_q}(t)$, in a globally asymptotic exponential dominated manner.

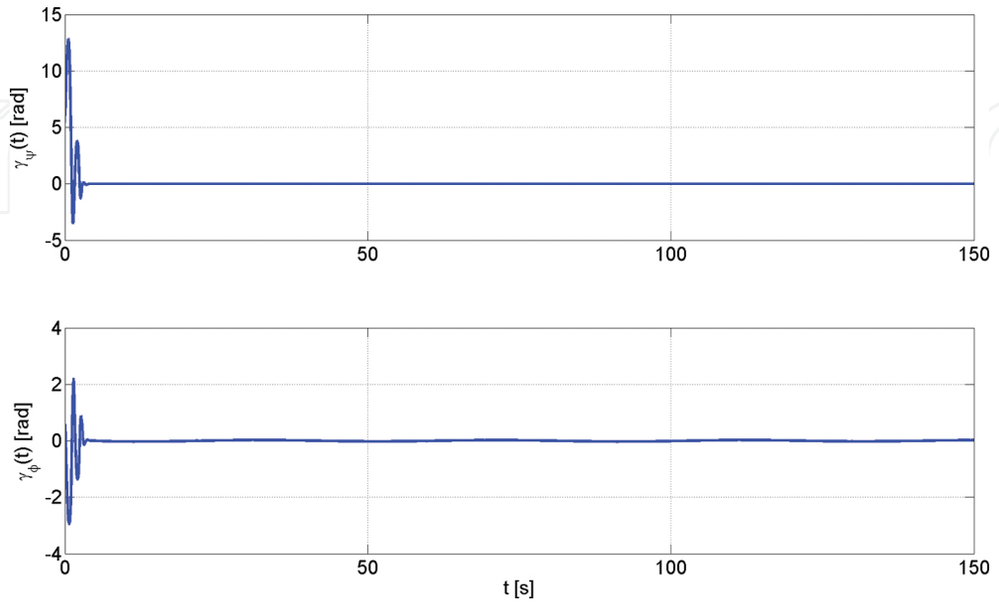

Figure 8. Evolution of the auxiliary control input vector of the mechanical multivariable PD controller, $\boldsymbol{\gamma}_m(t) = \left[\gamma_\psi(t), \gamma_\phi(t)\right]^T$.

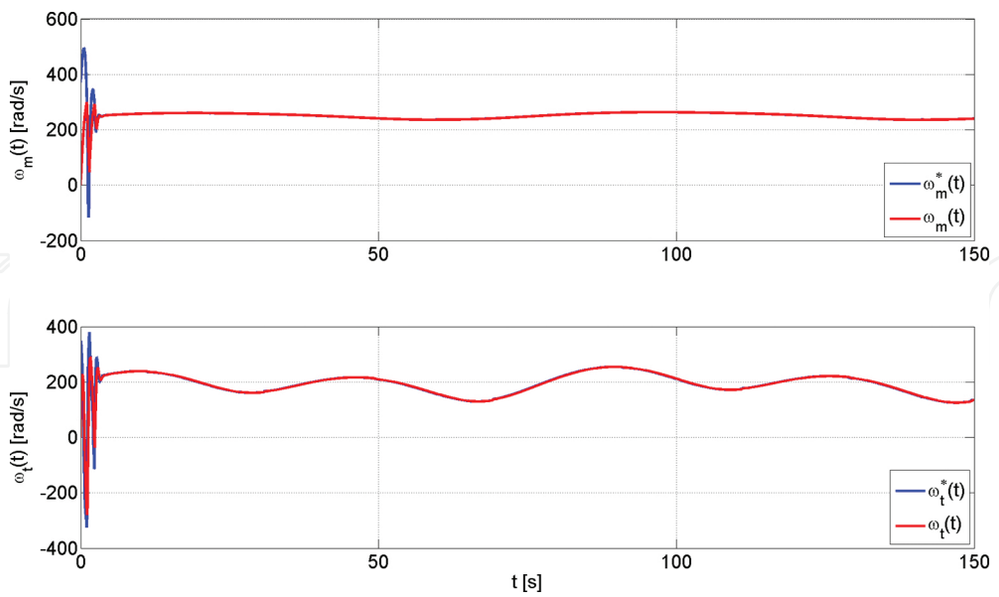

Figure 9. Real and desired evolution trajectories of the angular velocity vector, $\boldsymbol{\omega}^*(t) = \left[\omega^*_m(t),\ \omega^*_t(t)\right]^T$ and $\boldsymbol{\omega}(t) = \left[\omega_m(t),\ \omega_t(t)\right]^T$.

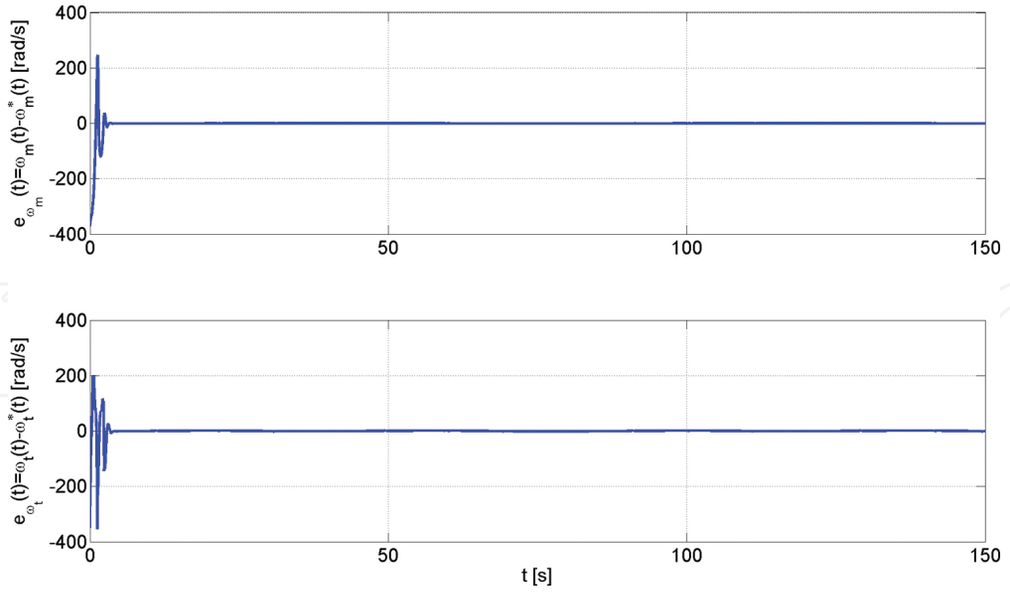

Figure 10. Evolution of the angular velocity error vector, $e_{\omega}(t) = \omega(t) - \omega^*(t) = [\omega_m(t) - \omega_m^*(t), \omega_t(t) - \omega_t^*(t)]\, T$.

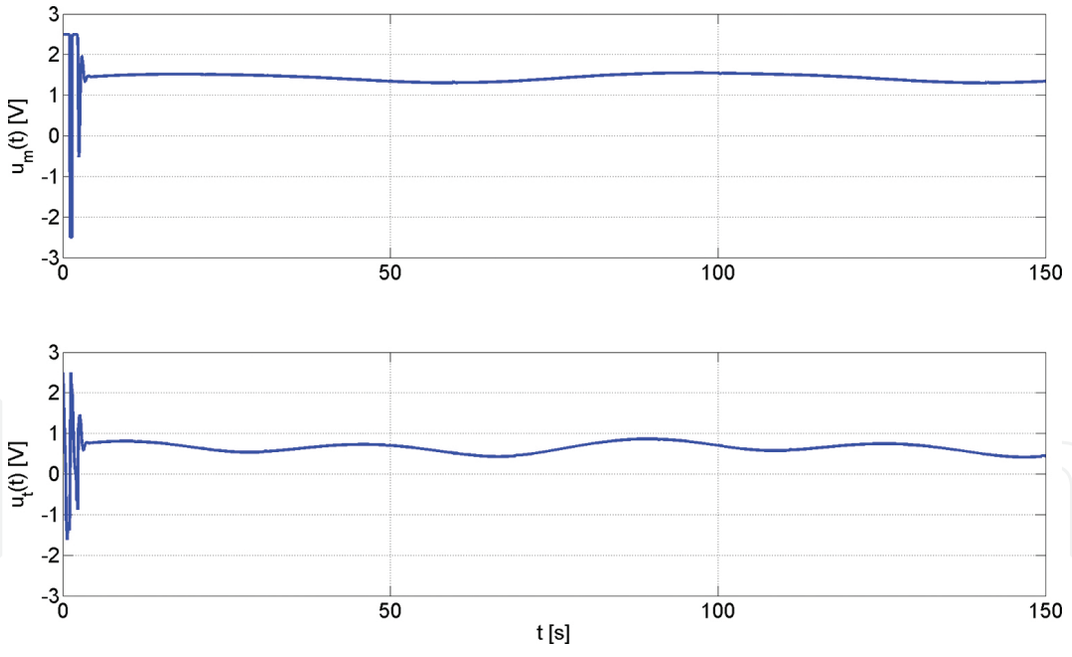

Figure 11. Evolution of the input voltage vector of the TRMS, $\boldsymbol{u}(t) = \left[u_m(t),\, u_t(t)\right]^T$.

On the other hand, the efficiency of the inner loop control (electrical controller) is depicted in **Figure 9**, including a comparative between the reference angular velocity vector, $\boldsymbol{\omega}^*(t) = \left[\omega_m^*(t), \omega_t^*(t)\right]^T$, obtained from the output of the outer loop, and the real magnitudes

http://dx.doi.org/10.5772/64875

of angular velocity vector, $\boldsymbol{\omega}(t) = \left[\omega_m(t), \omega_t(t)\right]^T$. The evolution of the angular velocity error vector, $\boldsymbol{e_\omega}(t) = \boldsymbol{\omega}(t) - \boldsymbol{\omega}^*(t) = \left[\omega_m(t) - \omega_m^*(t), \omega_t(t) - \omega_t^*(t)\right]^T$, is also shown in **Figure 10**.

To conclude this section, the input voltages in the MATLAB®/Simulink® environment, $\boldsymbol{u}(t) = \left[u_m(t), u_t(t)\right]^T$, for the main and tail rotors, are represented in **Figure 11**. From these graphs, it can be observed that the proposed control scheme has been realised to avoid saturations on these voltages, which in the simulation MATLAB®/Simulink® environment have been set to ± 2.5 V (similarly to the real prototype platform).

5. Conclusions

In this research, a novel nonlinear cascade-based control has been developed for the TRMS platform. The performance of the controller shows very satisfactory results in terms of convergence of the tracking errors for the generalised coordinates of the TRMS to a small neighbourhood to zero, smooth transient responses, low control efforts and robustness against large initial errors and parametric uncertainties in the model. The proposed control is an important base for the subsequent design of novel robust control algorithms in UAV platforms, which interest is notably increasing in recent years thanks to their multiple possibilities and applications. This will be the topic of our future research.

Acknowledgements

This work has been partially supported by Spanish Ministerio de Economía y Competitividad/FEDER under TEC2016-80986-R, DPI2016-80894-R, TIN2013-47074-C2-1-R and DPI2014-53499-R grants. Lidia M. Belmonte holds an FPU Scholarship (FPU014/05283) from the Spanish Government.

Author details

Lidia María Belmonte[1], Rafael Morales[1*], Antonio Fernández-Caballero[1] and José Andrés Somolinos[2]

*Address all correspondence to: Rafael.Morales@uclm.es

1 University of Castilla-La Mancha, School of Industrial Engineering, Albacete, Spain

2 Polytechnic University of Madrid, School of Naval Engineering, Madrid, Spain

References

[1] Castillo P., Lozano R., Dzul A.E. Modelling and control of mini-flying machines. London: Springer; 2005. doi:10.1007/1-84628-179-2

[2] Raffo G.V., Ortega M.G., Rubio F.R. An integral predictive/nonlinear H_∞ control structure for a quadrotor helicopter. Automatica. 2010; 46(1):29–39. doi:10.1016/j.automatica.2009.10.018

[3] Cai G., Chen B.M., Dong X., Lee T.H. Design and implementation of a robust and nonlinear flight control system for an unmanned helicopter. Mechatronics. 2011; 21(5): 803–820. doi:10.1016/j.mechatronics.2011.02.002

[4] Fernández-Caballero A., Belmonte L.M., Morales R., Somolinos J.A. Generalized proportional integral control for an unmanned quadrotor system. International Journal of Advanced Robotic Systems. 2015; 12(85): 1–14. doi:10.5772/60833

[5] Feedback Co. Twin rotor MIMO system 33-220 user manual. 1998

[6] Mullhaupt P., Srinivasan B., Lévine J., Bonvin D. A toy more difficult to control than the real thing. In: Proceedings of the European Control Conference (ECC'97). Brussels, July 1997

[7] Ahmad S.M., Chipperfield A.J., Tokhi M.O. Parametric modelling and dynamic characterization of a two-degree-of-freedom twin-rotor multi-input multi-output system. Proceedings of the Institution of Mechanical Engineers Part G, Journal of Aerospace Engineering. 2001; 215(2):63–78. doi:10.1243/0954410011531772

[8] Ahmad S.M., Shaheed M.H., Chipperfield A.J., Tokhi M.O. Non-linear modelling of a one-degree-of-freedom twin-rotor multi-input multi-output system using radial basis function networks. Proceedings of the Institution of Mechanical Engineers Part G, Journal of Aerospace Engineering. 2002; 216(4):197–208.doi: 10.1243/09544100260369731

[9] Shaheed M.H. Feedforward neural network based non-linear dynamic modelling of a TRMS using RPROP algorithm. Aircraft Engineering and Aerospace Technology: An International Journal. 2005; 77(1):13–22. doi:10.1108/00022660510576000

[10] Rahideh A., Shaheed M.H. Mathematical dynamic modelling of a twin-rotor multiple input-multiple output system. Proceedings of the Institution of Mechanical Engineers Part I, Journal of Systems and Control Engineering. 2007; 221(1): 89–101. doi: 10.1243/09596518JSCE292

[11] Rahideh A., Shaheed M.H., Huijberts H.J.C Dynamic modelling of a TRMS using analytical and empirical approaches. Control Engineering Practice. 2008; 16(3): 241–259. doi:10.1016/j.conengprac.2007.04.008

[12] Toha S.F., Tokhi M.O. ANFIS modelling of a twin rotor system using particle swarm optimisation and RLS. In: Cybernetic Intelligent Systems (CIS), 2010 IEEE 9th International Conference on; 1–2 Sept. 2010. IEEE. doi:10.1109/UKRICIS.2010.5898130

[13] Tastemirov A., Lecchini-Visintini A., Morales R.M. Complete dynamic model of a twin rotor MIMO System (TRMS) with experimental validation. In: 39th European Rotorcraft Forum 2013 (ERF 2013); 3–6 Sept. 2013. Moscow, Russia. ISBN: 978-1-5108-1007-5

[14] Ahmad S.M., Chipperfield A.J., Tokhi M.O. Dynamic modelling and open-loop control of a twin rotor multi-input multi-output system. Proceedings of the Institution of Mechanical Engineers Part I, Journal of Systems and Control Engineering. 2002; 216(6): 477–496. doi:10.1177/095965180221600604

[15] Ahmad S.M., Chipperfield A.J., Tokhi M.O. Dynamic modelling and linear quadratic Gaussian control of a twin-rotor multi-input multi-output system. Proceedings of the Institution of Mechanical Engineers Part I, Journal of Systems and Control Engineering. 2003; 217(3):203–227. doi:10.1177/095965180321700304

[16] López-Martínez M., Rubio F.R. Longitudinal control for a laboratory helicopter via constructive approximate backstepping. IFAC Proceedings Volumes. 2005; 38(1):289–294. doi:10.3182/20050703-6-CZ-1902.00448

[17] López-Martínez M., Ortega M.G., Vivas C., Rubio F.R. Nonlinear L_2 control of a laboratory helicopter with variable speed rotors. Automatica. 2007; 43(4): 655–661. doi: 10.1016/j.automatica.2006.10.013

[18] Rahideh A., Bajodah A.H., Shaheed M.H. Real time adaptive nonlinear model inversion control of a twin rotor MIMO system using neural networks. Engineering Applications of Artificial Intelligence. 2012; 25(6):1289–1297. doi:10.1016/j.engappai.2011.12.006

[19] Tao C.W., Taur J.S., Chen Y.C. Design of a parallel distributed fuzzy LQR controller for the twin rotor multi-input multi-output system. Fuzzy Sets and Systems. 2010; 161(15): 2081–2103. doi:10.1016/j.fss.2009.12.007

[20] Reynoso-Meza, G., Garcia-Nieto S., Sanchis J., Blasco, F.X. Controller tuning by means of multi-objective optimization algorithms: a global tuning framework. IEEE Transactions on Control Systems Technology. 2013; 21(2): 445–458. doi:10.1109/TCST.2012.2185698

[21] Coelho J., Matos R., Lebres C., Santos V., Fonseca N.M., Solteiro E.J., Tenreiro J.A. Application of fractional algorithms in the control of a twin rotor multiple input-multiple output system. In: 6th European Nonlinear Dynamics Conference (ENOC 2008). June 30–July 4, 2008. Saint Petersburg, Russia

[22] Christensen R., Fogh N., Hansen R.H., Jensen M.S., Larse S., Paramanathan A. Modelling and control of a twin-rotor MIMO system. Technical report, Aalborg University, Denmark; 2006

[23] Ekbote A.K., Srinivasan N.S., Mahindrakar A.D. Terminal sliding mode control of a twin rotor multiple-input multiple-output system. IFAC Proceedings Volumes. 2011; 44(1):10952–10957. doi:10.3182/20110828-6-IT-1002.00645

[24] Rotondo D., Nejjari F., Puig V. Quasi-LPV modeling, identification and control of a twin rotor MIMO system. Control Engineering Practice. 2013; 21(6): 829–846. doi:10.1016/j.conengprac.2013.02.004

[25] Feedback Co. Twin Rotor MIMO system. Advanced Teaching Manual 1. Manual: 33-007-4M5 Ed01. 1998

[26] Son Y.I., Kim I.H., Choi D.S., Shim D. Robust cascade control of electric motor drives using dual reduced-order PI observer. IEEE Transactions on Industrial Electronics. 2015; 62(6): 3672–3682. doi:10.1109/TIE.2014.2374571

IntechOpen